Discharge−Flow Kinetics Measurements Using Intracavity Laser Absorption Spectroscopy†

P. Sheehy and J. I. Steinfeld*

Department of Chemistry, Massachusetts Institute of Technology, Cambridge, Massachusetts 02139

Received: June 16, 2004; In Final Form: October 26, 2004

Intracavity laser absorption spectroscopy ("ICLAS") has been demonstrated as a feasible detection method for trace species in a discharge flow tube. This implementation has been used to measure the rate of the reaction between atomic hydrogen and NO to form HNO in helium carrier gas. A reaction rate constant of $(4.3 \pm 0.4) \times 10^{-32}$ cm^6 molecule^{-2} s^{-1} at 295 K was measured for the reaction H + NO + M → HNO + M (M = He). The pressure and concentration range enabled by ICLAS detection has allowed us to limit reactive pathways that would inhibit the formation of HNO. The sensitivity of ICLAS, coupled with the versatility of the discharge flow technique, suggests that intracavity absorption spectroscopy will be a useful technique for kinetics measurements on free radicals and other reactive species.

1. Introduction

Trace amounts of reactive molecular free radicals play an integral role in the chemical properties of the atmosphere.[1] A principal objective of laboratory studies of free radicals is to obtain the spectroscopic and kinetic parameters necessary to understand their behavior in the atmosphere.[2] The high reactivity of free radicals and the difficulty in generating, and subsequently isolating, the radical for analysis present significant challenges to their detection. Absorption spectroscopy is a powerful technique for identifying and measuring the concentration of reactive species. One of the many implementations of this technique, time-resolved tunable diode laser absorption spectroscopy, has provided much valuable information about the production and decay of highly energetic, short-lived species.[3−5] Linear absorption spectroscopy possesses a fundamental limitation, however, which is that the absorbance given by the Beer−Lambert law[6]

$$A = -\ln(I/I_0) = \sigma N l_{\text{eff}} \tag{1}$$

is limited by the product of the absorption cross section σ, the number density of absorbers N, and the effective absorption path length l_{eff}. If either the cross section or species density is extremely small, then the achievable absorbance is likely to be too small to be easily detected above the background noise in the source and/or the detector. The latter constraint, viz., low number density, is frequently the case in measurements of free radical kinetics.

Cavity enhanced spectroscopy offers an approach to compensate low intrinsic absorbance by placing the sample of interest within the cavity of a laser. In the intracavity laser absorption spectroscopy (ICLAS)[7−11] experiment, light from a lasing medium reflects through the absorbing sample as many as 10^5 times, amplifying the absorbance of a weak absorber to a much greater extent than in traditional multipass absorption cells. The effective path length in the absorbing medium is given by

$$l_{\text{eff}} = (l/L)ct_{\text{g}} \tag{2}$$

where l is the absolute path length through the absorbing sample, L is the total cavity length, c is the speed of light, and t_{g} is the generation time in the ICLAS laser.

We have coupled our ICLAS system to a discharge-flow apparatus[12,13] and measured the formation kinetics of HNO from atomic hydrogen and nitric oxide as a test of kinetics using intracavity absorption spectroscopy (KICAS). The results indicate that KICAS will be a promising method for carrying out kinetics measurements on weakly absorbing species. A related technique, simultaneous kinetics and ring-down (SKaR) has recently been reported by Brown et al.[14] In the latter approach, the reaction being studied is enclosed in a Cavity Ring-Down cell which is optically coupled to a pulsed laser.

2. Experimental Section

The ICLAS system used in these experiments has been previously described.[15,16] A traveling-wave, ring configuration was utilized for these measurements (Figure 1a). The horizontally polarized output of a 15 W argon ion laser (Coherent INNOVA Sabre DBW15) pumped a 5 × 15 mm Brewster cut, Ti:sapphire rod (AM), situated between two spherical folding mirrors (FM1 and FM2). A VWR Scientific Products chiller was used to maintain a temperature of 13 °C for the Ti:sapphire rod. The pump beam was focused on the gain medium by a focusing lens (FL). A wedged, horizontal polarizer (P) and a Faraday rotator (FR) were inserted into the short arm of the cavity, between the first high reflector (HR1) and the crystal (AM). Two high reflectors (HR2 and HR3) are used to compensate for the rotation of polarized light induced by the Faraday rotator and to ensure a unidirectional, traveling-wave. The height of the second high reflector (HR2) is adjustable to optimize the compensation. The distance between HR3 and the output coupler (OC) make up the long arm of the cavity, including the sample cell.

The Ti:sapphire laser was continuously tunable between 700 and 1000 nm. The laser was operated around 750 nm to access the desired HNO transition. Both the high reflectors and the folding mirrors had better than 99.9% reflectivity, whereas the three output couplers had better than 98% reflectivity. Tuning within a given wavelength region was performed by rotating or translating a pellicle beam splitter inserted into the short arm of the cavity.

† Part of the special issue "George W. Flynn Festschrift".

* Corresponding author. E-mail: jisteinf@mit.edu.

10.1021/jp040431u CCC: $30.25
Published on Web 02/10/2005

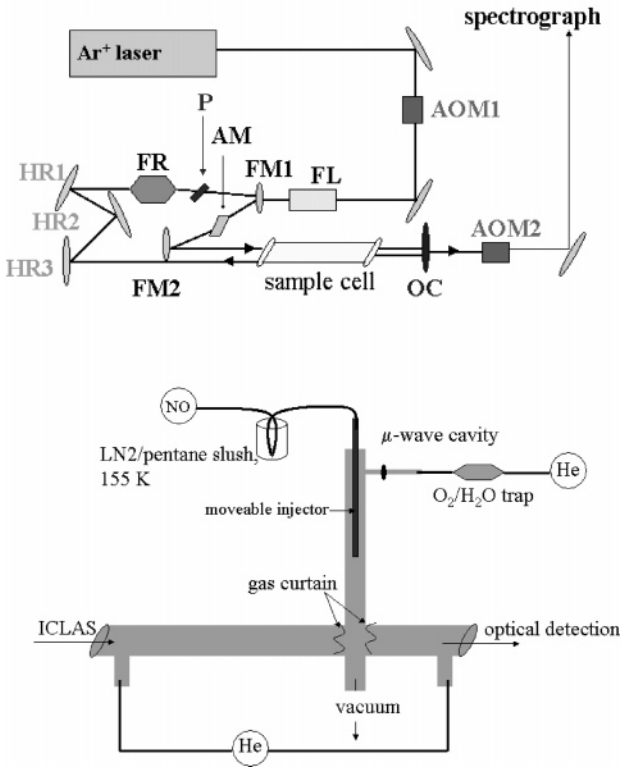

Figure 1. Apparatus for carrying out kinetics using intracavity absorption spectroscopy. (a) Traveling-wave, ring configuration of the ICLAS spectrometer. (b) Flow apparatus used for measuring HNO formation kinetics using the ICLAS spectrometer.

Large wedge windows with 2 in. diameter, 0.5 in. thickness, and a 1° wedge (CVI Laser Corp.) were used for the sample cells. The entire cavity of the laser, except for the sample cell, was housed within a constructed purge box. During experiments the box was purged with argon to remove residual absorbers, such as water and oxygen. The concentrations of these absorbers were reduced by 3 orders of magnitude.

The generation time of the laser was controlled by two acousto-optic modulators (AOM1 and AOM2). The first gate, AOM1 (IntraAction Corp. model ASM-802B39), directed the pump laser onto the Ti:sapphire gain medium, whereas the second gate, AOM2 (model ASM-40N), directed the output of the laser to the spectrograph. A 2.5 m echelle grating spectrograph dispersed the laser output, and the spectrally dispersed laser output was recorded with a linear silicon diode array (3,724 pixel Toshiba TCD1301D). The spectrograph could be operated in single, double, or triple pass mode by manually tilting the grating. Alignment of the spectrograph is performed with a 4 mW HeNe laser (Uniphase model 1057-0). The AOMs, the grating position, and the diode array were digitally controlled by software in Delphi programming language. The traveling-wave, ring configuration of the ICLAS laser resulted in effective path lengths of up to 3×10^4 km and detectable absorption coefficients on the order of 10^{-11} cm^{-1}.

The silicon linear diode array recorded a spectrum of photon count versus pixel number. The *x*-axis was calibrated for wavenumber and was linearized to account for the diffraction grating's wavelength-dependent dispersion. The *y*-axis was normalized to determine transmittance. The wavenumber calibration of ICLAS spectra was performed using nearby transitions from residual water or oxygen absorption lines. Although the cavity of the ICLAS laser was purged with argon, the path from the output coupler to the linear diode array detector was not purged. The 10 m path length between the output coupler and the diode array was sufficient to allow for the detection of both oxygen and water lines. Depending on the spectral region that the system was set up for, the known frequencies[17] of these lines were used to calibrate the spectra. In the case that the system was operated in a spectral region where oxygen and water absorption lines were insufficiently intense, an iodine absorption cell could be coupled with ICLAS to calibrate the spectra.[18]

The apparatus used for kinetic measurements is shown in Figure 1b. Experiments were carried out in a Pyrex tube (1.8 cm i.d., 65 cm long) connected to a T-cross that served as the axis for the optical detection system. Helium was used as the main carrier gas (BOC Gases, 99.999%). The flow tube gas was pumped by a Welch Duo-seal vacuum pump (500 L min^{-1}). Pressures were measured using a 0−100 Torr MKS Baratron manometer. The flow of the helium carrier gas was monitored using a TubeCube A7940HA-5 flow meter. The flow of nitric oxide was monitored using a Sierra Instruments Side Trak mass flow meter.

Hydrogen atoms were injected through a sidearm inlet located at the rear of the flow tube. The excess reactant, NO, was injected through a moveable inlet. The total flow through the injector was kept below 10% of the main carrier gas flow. Hydrogen, H_2, exists as a 1 ppm impurity in grade 5.0 helium.[19] The number density of the helium carrier gas is $\approx 10^{17}$ molecules cm^{-3}. This corresponds to a molecular hydrogen number density of $\approx 10^{11}$ molecules cm^{-3}. Atomic hydrogen was generated by passing the helium carrier gas through a microwave discharge. The microwave discharge cavity was cooled with a stream of nitrogen to maximize atomic hydrogen yields.[20] The helium was passed through an OxiClear Disposable Gas Purifier to effectively reduce the concentrations of water and oxygen. The efficiency of the microwave discharge cavity in dissociating molecular hydrogen may vary from day-to-day; however, regardless of potential day-to-day variations, between 1 and 10% of the molecular hydrogen should be atomized to generate H-atoms. This corresponds to $\approx 10^9-10^{10}$ molecules cm^{-3} of atomic hydrogen generated in the flow tube.

To remove NO_2, a purified stream of NO was prepared by passing the gas through a liquid nitrogen and pentane (LN_2/pentane) slush cooled to approximately 165 K. The temperature of the LN_2/pentane slush was monitored with a Fluke 51 Series II digital thermometer. Only a trace amount of NO_2 is necessary to affect the formation kinetics of HNO. The rate constant for the reaction between atomic hydrogen and NO_2 is several orders of magnitude greater than the HNO formation rate; so even though NO is present in excess, NO_2 still competes for hydrogen atoms. Minimizing, and essentially eliminating, NO_2 as an impurity is essential. Within the flow tube, the density of NO varied from 1×10^{16} to 3×10^{16} molecule cm^{-3}.

The ICLAS laser was constructed with Brewster surfaces to minimize losses. Two large wedge windows, 2 in. diameter, 0.5 in thick and a 1° wedge, were used for the sample cell. To prevent the diffusion of HNO into the sidearms, potentially contaminating the windows and decreasing the sample cell window transmission, a "gas curtain" of helium was introduced. Eliminating diffusion to the sidearms also eliminates the potential for inaccurate measurements of HNO number density as a result of an increased effective path length. The total flow rate was around 20 SLPM of air, corresponding to a linear flow rate of approximately 5×10^3 cm s^{-1}. Measurements were conducted at total pressures of both 13.85 and 24.00 Torr.

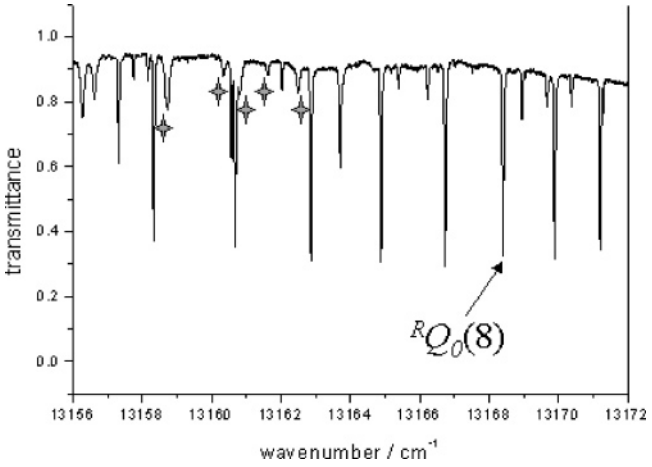

Figure 2. ICLAS spectrum of HNO used for kinetics measurements. The five transitions marked with a four-point star are oxygen absorption peaks that are used for frequency calibration of the spectrum.

3. HNO Spectroscopy

Nitrosyl hydride, HNO, was chosen to demonstrate the capability of ICLAS to measure kinetics in a discharge flow system. The HNO molecule was selected for a variety of reasons—it is a key intermediate in number of reactions relevant to the fields of astrophysics, combustion chemistry, and atmospheric chemistry.[21−26] HNO has a strong electronic transition within the spectral range of the Ti:sapphire-based ICLA Spectrometer. The molecule has a large absorption cross-section − requiring only trace amounts of HNO to conduct the necessary experiments ($\sigma > 10^{-17}$ cm^2 molecule^{-1}). In a setup with an occupation ratio of ∼35% and a generation time of 500 μs, a detection limit for HNO of ∼10^7 molecules cm^{-3} is achievable with ICLAS.

The spectroscopy of HNO has been measured extensively by both absorption[27−29] and emission methods.[30−32] The molecule has a bent equilibrium geometry and C_s symmetry in its three lowest lying electronic states: $\tilde{X}^1A'$, $\tilde{A}^1A''$, and $\tilde{a}^3A''$. HNO is a slightly asymmetric near prolate rotor ($\kappa = -0.988$). Only c-type transitions have been observed for the $\tilde{A} \leftarrow X$ transition, indicating the transition moment is perpendicular to the plane of the molecule. Kinetic measurements of HNO were made using the (000) ← (000) band of the $\tilde{A}^1A'' \leftarrow \tilde{X}^1A'$ electronic transition, centered at 13 154.38 cm^{-1}. The $^{R}Q_0(8)$ line of the $\Delta K_a'' = 0$ subband at approximately 13 168 cm^{-1} was used most often for monitoring HNO kinetics because of the lack of interference from other HNO lines and oxygen transitions, as well as sufficient oxygen at nearby frequencies to accurately calibrate the transition (Figure 2). Several other spectral lines in the $\Delta K_a'' = 1$ subband were interrogated and yielded kinetic plots essentially similar to those presented; because the $\Delta K_a'' = 1$ subband lies in a region in which there are no nearby oxygen calibration lines, the $\Delta K_a'' = 0$ subband was chosen for detailed measurements.

The absorption cross-section of the $^{R}R_3(6)$ transition of the (100) ← (000) band of HNO is reported in the literature as 3.3 × 10^{-20} cm^2 molecule^{-1} at room temperature.[33] Using known Franck−Condon factors[34] and rotational line strength factors calculated using expressions derived by Lide,[35] the absorption cross-section of the $^{R}Q_0(8)$ transition of the (000) ← (000) band of HNO was calculated to be 4.2 × 10^{-17} cm^2 molecule^{-1}, with an uncertainty of approximately 20%. This calculated cross-section provided the means to determine the number density of HNO for kinetic measurements.

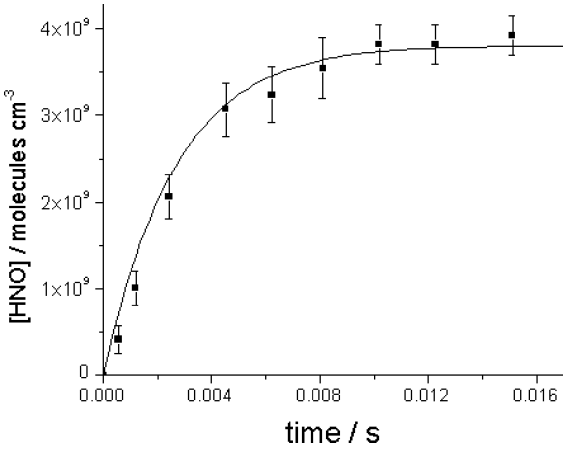

Figure 3. Sample kinetic plot at 13.85 Torr total pressure showing measured HNO number densities and a pseudo-first-order fit to the data. Error bars represent one standard deviation.

4. H + NO + M Kinetics

The following reactions are relevant to the study of HNO formation using ICLAS as the detection method:

$$H + NO + M \xrightarrow{k_1} HNO + M \quad \text{(R1)}$$

$$H + H + M \xrightarrow{k_2} H_2 + M \quad \text{(R2)}$$

$$HNO + H \xrightarrow{k_3} H_2 + NO \quad \text{(R3)}$$

$$HNO + \text{wall} \xrightarrow{k_w} \text{decay} \quad \text{(R4)}$$

The procedure used for determining the rate of reaction (R1) with this method is similar to that commonly used for low-pressure flow tubes;[12,13] however, the product, rather than reacting species, is monitored. Nitric oxide and helium were injected at a fixed rate, and their number densities were calculated assuming complete mixing in the region downstream of the injector. In each reaction, both NO and He (carrier gas = M) were present in several orders of magnitude greater than the estimated hydrogen atom concentration, creating pseudo-first-order conditions. The plasma discharge was initiated or "lit" and the position of the moveable injector was varied to generate a series of kinetic curves; an example is shown in Figure 3. A nonlinear least-squares fit was then performed in Microcal Origin. The data were fit to the following expression:

$$[HNO]_t = \frac{k_{eff}[H]_o}{k_w - k_{eff}}(e^{-k_{eff}t} - e^{-k_w t}) \quad (3)$$

where $k_{eff} = k_1[NO][M]$ (M = He), and $[H]_o$ is the initial concentration of atomic hydrogen in the flow tube in the absence of nitric oxide. The initial concentration of atomic hydrogen was not explicitly determined. The input value for $[H]_o$ was assumed to be approximately equal to $[HNO]_{z\ max}$ where z is the distance between the injector and the ICLAS axis of detection. When z was maximized, neither an increase in background pressure nor an increase in the concentration of NO yielded a higher concentration of HNO. Both of these indicators confirm that $[HNO]_{maximum} \approx [HNO]_{z\ max}$. It was also assumed that all the [HNO] formed at z_{max} was from the titration of atomic hydrogen with nitric oxide. This assumption leads to $[HNO]_{max} \approx [H]_o$. The number densities calculated for [HNO] are in good agreement with expected values: the concentration

of atomic hydrogen generated from the discharge was estimated between 10^9-10^{10} molecules cm^{-3} and the calculated number densities for $[HNO]_{max}$ vary between 3 and 5×10^9 molecules cm^{-3}.

Considering potential systematic errors in the measurement of gas flows, pressure, and detector signal, as well as uncertainties associated with the Franck−Condon factors used to calculate the HNO number density, it is estimated that the rate constant can be determined with an accuracy of ±20%.

The termolecular rate constant reported in Table 1 is $(4.3 \pm 0.4) \times 10^{-32}$ cm^6 $molecule^{-2}$ s^{-1}. Clyne and Thrush[36] and Miyazaki and Takahashi[37] have determined the value of k_1 by measuring the decrease in HNO emission intensity in a discharge-flow system. They report values of $(1.8 \pm 0.3) \times 10^{-32}$ and 3.0×10^{-32} cm^6 $molecule^{-2}$ s^{-1}, respectively. These are the only two values in the literature that report the formation of HNO with helium as a carrier gas. The work of Miyazaki and Takahashi requires a complicated data reduction scheme,[37] making a comparison of values extremely difficult.

Although similar concentrations of nitric oxide were used in all experiments, the concentration of atomic hydrogen in the previous work was approximately 0.5−2% of the total flow.[36−39] In this work, the concentration of atomic hydrogen was reduced to approximately 1×10^{-4}% of the total flow. Minimizing the concentration of atomic hydrogen limits the potential for other formation or recombination reactions involving atomic hydrogen. Similarly, limiting the concentration of atomic hydrogen limits the formation of HNO. This prevents potential losses of HNO via wall loss, self-reaction, or other successive reactions.

In the KICAS flow tube, the absorption spectrum of HNO is not observed if the nitric oxide stream is not purified by means of the LN2/pentane cold bath. Nitrogen dioxide exists as an impurity in the stream of NO from the cylinder. Nitrogen dioxide reacts much faster with atomic hydrogen than nitric oxide does. A rigorous purification of the NO stream is essential to measuring the rate parameters of (R1) and (R4) accurately. Clyne and Thrush make a similar observation in that they are unable to detect the "glow intensity" due to the emission of HNO at increased concentrations of nitrogen dioxide.[36]

The work of Clyne and Thrush[36,38] neglects to account for any potential wall loss—for both HNO and atomic hydrogen. In our system, it is possible that the wall is acting as a third body and contributing to the stabilization of the electronically excited HNO* molecule, as well as acting as a loss site. Similar recombination phenomena are possible with atomic hydrogen. The only indication of sensitivity to detecting HNO in the literature is given by observations associated with the steady-state concentration of HNO being much less than 0.2[NO].[36,38] A rough estimate of the detection sensitivity reveals that the HNO was observed in concentrations around $10^{12}-10^{13}$ molecules cm^{-3}, much higher than the concentrations reported here. In the present work, we effectively reduced the concentration of HNO so that we could isolate the formation of HNO, followed by a slow wall reaction. At higher concentrations of HNO, it is unlikely that the slow self-reaction,

$$HNO + HNO \rightarrow H_2O + N_2O \qquad (R5)$$

becomes significant; however, it is likely that higher concentrations of HNO will affect the fast reaction,

$$HNO + H \rightarrow H_2 + NO \qquad (R3)$$

Although (R3) is and should be considered in the study by Clyne and Thrush,[36] the potential of this reaction to skew the measured concentration of HNO in the ICLAS system is minimized by manipulating the number densities and flows such that [NO] ≫ [H], [HNO].

TABLE 1: Observed Termolecular Rate Constants at 13.85 and 24.00 Torr for the Reaction

$$H + NO \xrightarrow{M} HNO$$

pressure, Torr	velocity, 10^3 cm s^{-1}	$[H]_o$, 10^9 cm^{-3}	$k_1 \pm \sigma$, 10^{-32} cm^6 s^{-1}	$k_{wall} \pm \sigma$, s^{-1}
13.85	5.3	4.15	3.0 ± 0.3	0.6 ± 0.3
	4.9	4.01	4.1 ± 0.4	0.5 ± 0.4
24.00	5.1	3.86	5.7 ± 0.4	0.7 ± 0.2
	5.1	3.92	4.7 ± 0.5	0.7 ± 0.4
	5.2	4.01	4.1 ± 0.4	0.5 ± 0.5

The total pressure in the system employed by Clyne and Thrush was 5−10 times lower than the pressures used in this experiment. Under the experimental conditions reported by Clyne and Thrush, it is interesting to note that $k_3 > k_2[M]$. This is not the case in our experiment. By limiting the concentration of atomic hydrogen and the formation of HNO, we were able to observe a steady-state concentration of HNO (at about 6 ms of reaction time).

The wall loss reaction is reported with high uncertainties because of the relatively small effect it has on the simulated curve (vide infra) up to a value of 1 s^{-1}. The upper limit for the rate constant of the wall reaction for this system is reported as 1 s^{-1}, and is most likely in the range 0.2−0.7 s^{-1}, which is in good agreement with other reported values.[40,41] At values above 1 s^{-1}, the curve fitting function, eq 3, begins to demonstrate behavior inconsistent with the experimental observations. On the time scale of the experiment (∼20 ms), a value greater than 1 s^{-1} would demonstrate a slow, but detectable decline in the concentration of HNO. All of the experimental data at varying pressures observed here supports a slower decay associated with the wall reaction.

The Aurora application, part of the CHEMKIN software package,[42] simulates the time evolution or steady state of a well mixed reactor. The Aurora application was used to model the series of reactions ((R1)−(R4)) in the HNO reaction system to compare numerically modeled kinetics curves with the experimental curves obtained from the KICAS measurements.

The rates used in the simulations were: $k_1 = 4.3 \times 10^{-32}$ cm^6 $molecule^{-2}$ s^{-1}, $k_2 = 6 \times 10^{-33}$ cm^6 $molecule^{-2}$ s^{-1}, $k_3 = 1.7 \times 10^{-12}$ $cm^3 molecule^{-1}$ and $k_w = 0.5$ s^{-1}. The application was run under conditions appropriate to the experiments reported above. The simulated kinetics curves showed good agreement with the experimental data.[43]

5. Discussion

ICLAS has been demonstrated as a feasible detection method for trace species in a discharge flow tube. This implementation has been used to measure the rate of the reaction between atomic hydrogen and NO to form HNO in helium carrier gas. A reaction rate constant of $(4.3 \pm 0.4) \times 10^{-32}$ cm^6 $molecule^{-2}$ s^{-1} at 295 K was measured for the reaction H + NO + M → HNO + M (M = He). The pressure and concentration range enabled by ICLAS detection has allowed us to limit reactive pathways that would inhibit the formation of HNO. The sensitivity of ICLAS, coupled with the versatility of the discharge flow technique, suggests that intracavity absorption spectroscopy will be a useful technique for kinetics measurements on free radicals and other reactive species.

The KICAS method described here is essentially equivalent to similar methodologies used in kinetic studies employing

cavity ring down spectroscopy in a pulsed-photolysis or discharge-flow configuration. The primary difference between KICAS and CRDS-based experiments is the accessible spectral range of the spectroscopic system employed. The SKaR method recently reported by Brown et al.[14] represents an analogous methodology. The sensitivity of both SKaR and KICAS are comparable. One specific advantage that KICAS or a conventional configuration for CRDS detection may have over SKaR is the time scale accessible for kinetic measurements, as SKaR is inherently limited by the empty cavity time constant (τ_0) which the authors state is variable up to hundreds of microseconds. To be a candidate for SKaR, a reaction must have kinetics on the order of τ_0. The experiment reported here was carried out at time scales up to 20 ms, well beyond the range of SKaR. On the other hand, SKaR is an attractive option for kinetics experiments at short time scales, as a laser light pulse into the cavity initiates the experiment and controls the time scale, whereas KICAS requires a more complicated discharge flow configuration to operate at shorter time scales. Both methodologies have their merit, and should be considered complementary.

Acknowledgment. This work was supported by NASA Upper Atmosphere Research program grant NAG5-10613. P.S. gratefully acknowledges the award of a Fellowship from the Martin Family Society of Fellows for Sustainability. Dr. A. A. Kachanov and S. Witonsky provided helpful advice on setting up and operating the ICLAS instrument; Dr. M. Hunter and K. Broekhuizen of the Molina Group at MIT. provided important assistance in setting up and operating the discharge flow system.

References and Notes

(1) Seinfeld, J. H.; Pandis, S. N. *Atmospheric Chemistry and Physics: From Air Pollution to Climate Change*; Wiley: New York, 1998.
(2) Lightfoot, P. D.; Cox, R. A.; Crowley, J. N.; Destriau, M.; Hayman, G. D.; Jenkin, M. E.; Moortgat, G. K.; Zabel, F. *Atmos. Environ. Part A − Gen. Top.* **1992**, *26*, 1805.
(3) Sedlacek, A. J.; Weston, R. E., Jr.; Flynn, G. W. *J. Chem. Phys*. **1991**, *94*, 6483.
(4) Hewitt, S. A.; Zhu, L.; Flynn, G. W. *J. Chem. Phys*. **1992**, *97*, 6396.
(5) Mullin, A. S.; Michaels, C. A.; Flynn, G. W. *J. Chem. Phys*. **1995**, *102*, 6032.
(6) Beer, A. *Ann. Phys.* **1852**, *86*, 78.
(7) Pakhomycheva, L. A.; Sviridenkov, E. A.; Suchkov, A. F.; Titova, L. V.; Chrilov, S. S. *JETP Lett*. **1970**, *12*, 43.
(8) Peterson, A. *J. Opt. Soc. Am*. **1971**, *61*, 746.
(9) Hänsch, T. S.; Schawlow, A. L.; Toschek, P. E. *IEEE J. Quantum Electron.* **1972**, *8*, 802.
(10) Kachanov, A. A.; Charvat, A.; Stoeckel, F. *J. Opt. Soc. Am. B* **1994**, *11*, 2412.
(11) Campargue, A.; Stoeckel, F.; Chenevier, M. *Spectrochim. Acta Rev.* **1990**, *13*, 69.
(12) Howard, C. J. *J. Phys. Chem*. **1979**, *83*, 3.
(13) Seeley, J. V.; Jayne, J. T.; Molina, M. J. *J. Phys. Chem*. **1996**, *100*, 4019.
(14) Brown, S. S.; Ravishankara, A. R.; Stark, H. *J. Phys. Chem. A* **2000,** *104*, 7044.
(15) Yang, S.f.; Canagaratna, M. R.; Witonsky, S. K.; Coy, S. L.; Steinfeld, J. I.; Field, R. W.; Kachanov, A. A. *J. Mol. Spectrosc.* **2000**, *201*, 188.
(16) Witonsky, S. K.; Canagaratna, M. R.; Coy, S. L.; Steinfeld, J. I.; Field, R. W.; Kachanov, A. A. *J. Chem. Phys.* **2001**, *115*, 3134.
(17) Rothman, L. S.; Rinsland, C. P.; Goldman, A.; Massie, S. T.; Edwards, D. P.; Flaud, J. M.; Perrin, A.; Camy-Peyret, C.; Dana, V.; Mandin, J. Y.; Schroeder, J.; McCann, A.; Gamache, R. R.; Watson, R. B.; Yoshino, K.; Chance, K. V.; Jucks, K. W.; Brown, L. R.; Nemtchinov, V.; Varanasi, P. *J. Quant. Spectrosc. Rad. Transfer* **1998**, *60*, 665.
(18) Gerstenkorn, S.; Luc, P.; Verges, J. *Atlas du Spectre d'Absorption de la Molecule d'Iode: 7200−11200 cm*$^{-1}$, CNRS: Paris, 1993.
(19) Private communication from J. Jordan, BOC Gases Inc.
(20) Stonge, L.; Moisan, M. *Plasma Chem. Plasma Proc*. **1994**, *14*, 87.
(21) DeMore, W. B.; Sander, S. P.; Golden, D. M.; Hampson, R. F.; Kurylo, M. J.; Howard, C. J.; Ravishankara, A. R.; Kolb, C. E.; Molina, M. J. *Chemical Kinetics and Photochemical Data for Use in Stratospheric Modeling*; JPL: Pasadena, CA, 1997; Publication 97-4.
(22) Graedel, T. E.; Langer, W. D.; Frerking, M. A. *Astrophys. J. Supp. Ser*. **1982**, *48*, 321.
(23) Viala, Y. P. *Astron. Astrophys. Supp. Ser*. **1986**, *64*, 391.
(24) Miller, J. A.; Bowman, C. T. *Prog. Energy Combust. Sci.* **1989**, *15*, 287.
(25) Soto, M. R.; Page, M.; McKee, M. L. *Chem. Phys. Lett*. **1991**, *187*, 335.
(26) Viereck, R. A.; Bernstein, L. S.; Mende, S. B.; Murad, E.; Swenson, G. R.; Pike, C. P. *J. Spacecraft Rockets* **1993**, *30*, 724.
(27) Dalby, F. W. *Can. J. Phys.* **1958**, *36*, 1336.
(28) Bancroft, J. L.; Hollas, J. M.; Ramsay, D. A. *Can. J. Phys*. **1962**, *40*, 322.
(29) Johns, J. W. C.; McKellar, A. R. W. *J. Chem. Phys*. **1977**, *66*, 1217.
(30) Dixon, R. N.; Noble, M.; Taylor, C. A.; Delhoume, M. *Discuss. Faraday Soc*. **1981**, *71*, 125.
(31) Dixon, R. N.; Jones, K. B.; Noble, M.; Carter, S. *Mol. Phys*. **1981**, *42*, 455.
(32) Obi, K.; Matsumi, Y.; Takeda, Y.; Mayama, S.; Watanabe, H.; Tsuchiya, S. *Chem. Phys. Lett.* **1983**, *95*, 520.
(33) Cheskis, S. G.; Nadtochenko, V. A.; Sarkisov, O. M. *Int. J. Chem. Kinet.* **1981**, *13*, 1041.
(34) Mordaunt, D. H.; Flothmann, H.; Stumpf, M.; Keller, H. M.; Beck, C.; Schinke, R.; Yamashita, K. *J. Chem. Phys*. **1997**, *107*, 6603.
(35) Lide, D. R. *J. Chem. Phys*. **1952**, *20*, 1761.
(36) Clyne, M. A. A.; Thrush, B. A. *Discuss. Faraday Soc*. **1962**, *33*, 139.
(37) Miyazaki, S.; Takahashi, S. *Mem. Def. Acad. Jpn.* **1969**, *9*, 643.
(38) Clyne, M. A. A.; Thrush, B. A. *Trans. Faraday Soc*. **1961**, *57*, 1305.
(39) Hartley, D. B.; Thrush, B. A. *Proc. R. Soc. A* **1967**, *297*, 520.
(40) Bryukov, M. G.; Kachanov, A..A.; Timonnen, R.; Seetula, J.; Vandoren, J.; Sarkisov, O. M. *Chem. Phys. Lett*. **1993**, *208*, 392.
(41) Callear, A. B.; Carr, R. W. *J. Chem. Soc., Faraday Trans*. **1975**, *71*, 1603.
(42) Distributed by Reaction Design, Inc.
(43) P. Sheehy, Ph.D. Thesis, Massachusetts Institute of Technology, 2005.